Ultra-low coverage genome-wide association study - insights into gestational age using 17,844 embryo samples with preimplantation genetic testing

Shumin Li[1,#], Bin Yan[1,#], Thomas K.T. Li[6,#], Jianliang Lu[1], Yifan Gu[4,5], Yueqiu Tan[4,5], Fei Gong[4,5], Tak-Wah Lam[1], Pingyuan Xie[2,3,*], Yuexuan Wang[1,7,*], Ge Lin[3,4,5,*], Ruibang Luo[1,*]

[1] Department of Computer Science, The University of Hong Kong, Hong Kong, China
[2] Hunan Normal University School of Medicine, Changsha, 410013, Hunan, China
[3] National Engineering and Research Center of Human Stem Cell, Changsha, Hunan, China
[4] NHC Key Laboratory of Human Stem Cell and Reproductive Engineering, School of Basic Medical Science, Institute of Reproductive and Stem Cell Engineering, Central South University, Changsha 410008, Hunan, China
[5] Clinical Research Center for Reproduction and Genetics in Hunan Province, Reproductive and Genetic Hospital of CITIC-Xiangya, Changsha 410013, Hunan, China
[6] Department of Obstetrics & Gynecology, Queen Mary Hospital, The University of Hong Kong, Hong Kong, China
[7] College of Computer Science and Technology, Zhejiang University, Hangzhou, China

[#] These authors contributed equally to this work
[*] To whom correspondence should be addressed: Ruibang Luo, Email: rbluo@cs.hku.hk, Ge Lin, Email: linggf@hotmail.com, Yuexuan Wang, Email: amywang@hku.hk, Pingyuan Xie, Email：plainxie192@126.com

Abstract

Background: Very low coverage (0.1 to 1x) whole genome sequencing (WGS) has become a promising and affordable approach to discover genomic variants of human populations for Genome-Wide Association Study (GWAS). To support genetic screening using Preimplantation Genetic Testing (PGT) in a large population, the sequencing coverage goes below 0.1x to an ultra-low level. However, its feasibility and effectiveness for GWAS remains undetermined.

Methods: We devised a pipeline to process ultra-low coverage WGS data and benchmarked the accuracy of genotype imputation at the combination of different coverages below 0.1x and sample sizes from 2,000 to 16,000, using 17,844 embryo PGT with approximately 0.04x average coverage and the standard Chinese sample HG005 with known genotypes. We then applied the imputed genotypes of 1,744 transferred embryos who have gestational ages and complete follow-up records to GWAS.

Results: The accuracy of genotype imputation under ultra-low coverage can be improved by increasing the sample size and applying a set of filters. From 1,744 born embryos, we identified 11 genomic risk loci associated with gestational ages and 166 genes mapped to these loci according to positional, expression quantitative trait locus and chromatin interaction strategies. Among these mapped genes, *CRHBP, ICAM1* and *OXTR* were more frequently reported as preterm birth related. By joint analysis of gene expression data from previous studies, we constructed interrelationships of mainly

CRHBP, ICAM1, PLAGL1, DNMT1, CNTLN, DKK1 and *EGR2* with preterm birth, infant disease and breast cancer.

Conclusions: This study not only demonstrates that ultra-low coverage WGS could achieve relatively high accuracy of adequate genotype imputation and is capable of GWAS, but also provides insights into uncovering genetic associations of gestational age trait existed in the fetal embryo samples from Chinese or Eastern Asian populations.

Keywords: Ultra-low coverage Whole Genome Sequencing, Imputation, Single Nucleotide Polymorphisms, Genome-Wide Association Study, Gestational Age, Preterm Birth

Background

Detection and characterization of genetic variants associated with traits and diseases are fundamental to the study of human genetics. Genome-Wide Association Study (GWAS) is an approach widely used in genetic research that aims to decode the associations of specific genetic variations with particular diseases or traits in sample populations. In the past decade, GWAS has facilitated discovery of over one hundred thousand variants associated with complex traits in human (1). Whole-genome sequencing (WGS) has emerged as a dominant technology in GWAS because it enables one to generate a comprehensive view of the genomic variation landscape for not only a specific trait but also for common diseases. Thus, WGS-based approaches hold a significant advantage over genome-wide genotyping arrays or exome sequencing in the analysis of complete genetic variations. However, with a fixed budget, the high cost of sequencing many DNA samples is a limitation for GWAS (2-4). Recently, to reduce the cost of sequencing, a number of low (0.5-1x) or extremely low-coverage (0.1-0.5x) WGS has been carried out as an alternative method of genotyping (2, 5, 6). It is, however, unclear whether ultra-low coverage WGS (ulcWGS) below 0.1x data can capture enriched genetic variations across the entire allele frequency (AF) spectrum. When considering a balance between number of samples sequenced and sequencing read coverage, effective genotype imputation could provide more authentic DNA variants that would be helpful for genetic research.

Genotype imputation can be used to infer missing genotypes and to increase the accuracy of detecting genetic variants, such as single nucleotide polymorphisms (SNPs).

118 In general, performance of genotype imputation is largely affected by sample size,
119 sequencing coverage, analysis methods, and other parameters (7). A main challenge to
120 use very low coverage WGS is how to achieve an adequately accurate imputation for
121 downstream analyses. Previous attempts have shown the efficiency of low coverage
122 WGS, for example, a high r^2 of imputation accuracy observed by using 10 low coverage
123 WGS (~0.5x) as compared to known genotypes (6). Pasaniuc et al. reported that the
124 GWAS signals obtained from using 909 whole-exome sequencing (~0.24x) are
125 comparable to using genotyping array (2). Gilly et al. found that more true association
126 signals were identified by WGS (~1.0x) than the traditional array-based study (5).
127 Using ulcWGS (0.06x-0.1x) with 141,431 samples from a Chinese genomic study, the
128 accuracy of imputed genotypes reached 0.71 (8). Even though the distribution of
129 genetic background from large number of samples is expected to compensate for the
130 low sequencing coverages, it has never been determined how many samples are needed
131 to achieve a relatively high accuracy. More importantly, lack of comparative data with
132 coverages less than 0.05x results in the limited application of ulcWGS to GWAS.

133 Gestational age is an important complex trait associated with biological processes
134 and human disease. Biologically, gestational duration plays a vital role in both mental
135 and physical health of children at an age of five-year-old (9). Gestational age shorter
136 than 37 weeks is categorized as Preterm Birth (PTB). Previous studies found the
137 contribution of both the maternal and fetal genomes to variation of gestational ages (10-
138 12). However, they focused on European and African samples by involving few
139 samples from Chinese or Eastern Asian ancestries. Overall, biological mechanisms

140 underlying variation of gestational durations remain unclear, primarily because
141 insufficient maternal or fetal genotypes with widespread gestational ages have been
142 collected (13). Recently, Preimplantation Genetic Testing (PGT) with trophectoderm
143 biopsy for embryo aneuploidy screening has become a common practice in *in vitro*
144 fertilization (14, 15), and poses as an expectant source of genotypes for GWAS.
145 However, if the average sequencing coverage of PGT is even lower than the lowest
146 levels that have been reported in GWAS so far, it is necessary to examine whether such
147 PGT datasets are appropriately applied to GWAS.

148 In this study, we devised a pipeline for analyzing and applying the ulcWGS of
149 17,844 embryo samples for GWAS. Our result shows that a large sample size is
150 effective to increase the accuracy of genotype imputation even at an ultra-low coverage.
151 Furthermore, using the imputed genotypes of 1,744 embryos that were successfully
152 transferred and born with a widespread of gestational ages, we demonstrate the power
153 of using ulcWGS in GWAS and provides insights into understanding genetic
154 association of gestational age in embryos acquired from Chinese and East Asians.
155 Refreshing the lowest coverage used in GWAS, our finding also provides a foundation
156 for exploring the utilization of an even lower coverage for dissecting genotype-
157 phenotype associations.
158

159 # Methods

160 ## Samples and sequencing coverage

161 The whole PGT dataset of 17,844 embryos was from the Clinical Research Center for
162 Reproduction and Genetics in Hunan Province, Reproductive and Genetic Hospital of

163 China International Trust Investment Corporation - Xiangya. The protocol of embryo
164 culture and biopsy was published in a related study (16). Three WGA kits were applied
165 to the biopsied TE cells by following the manufactures' guides, including REPLI-g
166 Mini Kit (called MDA), WGA4 GenomePlex Single Cell Whole Genome
167 Amplification Kit (called dop-PCR) and Rubicon Genomics PicoPlex Single Cell
168 Whole Genome Amplification Kit (called PicoPlex). A 1-2 μg of the WGA product was
169 subjected to library construction and sequencing on the four platforms, including BGI-
170 Seq 500, Illumina MiSeq, Ion Proton, Ion Torrent (Additional file 1: Table S2).
171

172 **Study design**

173 We developed a three-step pipeline to carry out genotype imputation using ulcWGS
174 data and to perform GWAS of the detected SNPs (Fig. 1). Firstly, the raw reads of the
175 17,844 embryo samples were aligned to the hs37d5 reference genome. Sequencing
176 coverage of these embryo samples displays a distribution with an average coverage
177 0.04x (Additional file 3: Figure S1). To our best knowledge, it is below the coverage of
178 any dataset used previously for genotype imputation. After removing potential PCR
179 duplicates, the aligned reads were used to call population SNPs. Secondly, we
180 conducted genotype imputation on each individual sample at the called population
181 SNPs and assessed the genotyping accuracy based on the standard Chinese sample
182 HG005 with known genotypes from GIAB (Genome in a Bottle, NIST)(17). Last, we
183 applied the imputed genotypes from 1,744 born embryos with complete follow-up

records to GWAS and explored biological associations between the genetic variants detected in the born embryos and their gestational ages.

Sequencing read processing and alignment

In the first step of Fig. 1, the raw reads of the PGT samples were delivered in two types, fastq or BAM. For BAM data, we used bedtools (18) to extract the raw reads into single-end fastq files. The raw reads of each sample were then aligned to the hs37d5 reference genome using BWA (19). BWA-mem was applied to samples sequenced by the Ion Torrent with longer reads and "bwa aln" was used for the rest of the samples with shorter reads. Samtools rmdup (20) was used to remove the potential PCR duplicates.

Population SNP calling

In the population SNP calling stage, we modified the method of Liu et al. (8). The first stage is to use log-likelihood estimation for AF estimation, and the second stage is to use log-likelihood ratio test for determining allelic types. More details are described in Additional file 2: Supplementary Methods.

SNP calls of the raw population were filtered following the rules, 1) calls that overlapped with the 35-kmer problematic alignment regions in hs37d5 were removed (21); 2) calls that overlapped with regions with ENCODE mappability uniqueness score unequal to 1 were removed (22), tool "bigWigToBedGraph" used afterward to convert the bigwig into bed format) (23).

207 **Genotype imputation**

208 We used STITCH (24) version 1.5.7 for genotype imputation. The ancestral haplotypes
209 number *k* was set as 20, the assumed number of generations *nGen* was set to 2000, and
210 the reads were binned into windows with *gridWindowSize* 10000. The *diploid* mode in
211 STITCH was used. Although using a reference panel is optional in STITCH, we used
212 the IMPUTE2 1000 genome haplotypes phase 1 reference panel as it improves the
213 accuracy of imputation when the sample size is small. With sample size larger than
214 10,000, the improvement was not significant. All parameters were optimized by
215 maximizing the r^2 of the estimated AFs between imputation and population SNP
216 calling in a randomly chosen 5 Mbp genomic region (chr3:180-185Mbp). When
217 applying STITCH to the whole genome, we divided the genome into 5 Mbp windows
218 with a 500 Kbp overlap between two windows.

219 For benchmarking, seqtk was used to subsample the HG005 Illumina WGS raw
220 reads to 0.01x-0.1x (Paired-end 250bp, 300-fold). We aligned the reads to hs37d5 by
221 using the same pipeline as used in the embryo samples. Because a computer takes a few
222 years to impute whole genome with tens of thousands of samples, we worked on only
223 chromosome 1, the longest one in human. The genotype imputation was benchmarked
224 according to 80 combinations of the 10-scale coverages of HG005 with 8 sizes of our
225 samples from 2,000 to 16,000, respectively.

226 All bi-allelic SNPs with MAF ≥ 0.01 found in chromosome 1 with the population
227 SNP calling from the 17,844 samples are included for genotype imputation. We used
228 the 167,814 SNPs both in our SNP callset and HG005 known genotypes for

229 benchmarking. The imputed genotypes were compared to the truth released by GIAB
230 for estimating the imputation accuracy. Then, genotype imputation was applied to all
231 17,844 embryo datasets at the 31,622,332 bi-allelic sites with MAF ≥ 0.01 found in
232 population SNP calling. The entire imputation process spent 19 days and used 15
233 machines with 16 cores (two 8-core Intel Xeon Silver 4108 CPU). Two filters "INFO
234 score ≥ 0.4 and HWE *p*-value >1e-6" were applied to select the imputed genotypes.
235

236 **Genome-wide association study (GWAS)**

237 To conduct GWAS, we used score statistics (25) that is implemented in ANGSD (26).
238 Variants satisfying four conditions were selected as inputs, including 1) known in
239 dbSNP150, 2) MAF ≥ 0.01, 3) INFO score ≥ 0.4, and 4) HWE *p*-value > 1e-6. To
240 remove biases, we specified 16 covariates for ANGSD, 8 most significant principal
241 components calculated from the inputs of PCA (Additional file 2: Supplementary
242 Methods), and 8 clinical records including maternal age, maternal BMI, fetal sex, either
243 parent with single-gene disease, either parent with chromosome abnormality, multiple
244 pregnancy, preeclampsia and gestational diabetes of mellitus. Except the default
245 parameters, we set *minHigh* to 15 (requiring at least 15 high credible genotypes from
246 the input) instead of 10 to achieve better accuracy with a large sample size. ANGSD
247 did not create an output beta-coefficient, so we followed the ideas of Skotte et al. (25)
248 by incorporating the genotype probabilities and all 16 covariates into a linear regression
249 model, with the gestational age as a response variable. The effect size was calculated
250 by the coefficient of genotypes.

251 **Independent SNPs and genomic risk loci**

252 The significant SNPs from our GWAS were mapped to genomic risk loci using FUMA
253 pipeline (27) and the LD information of 1000G EAS variants (28). We first defined
254 "independent significant SNP", a SNP that meets genome-wide significance level
255 (p value $\leq 4.515e-8$) and is independent of other significant SNPs (with LD $r^2 <$
256 0.6). FUMA also generated a set of lead SNPs with low LD and with other ($r^2 < 0.1$)
257 from the independent significant SNPs. The genomic risk loci were identified by
258 starting from these lead SNPs and through iteratively merging related genomic regions
259 to them according to FUMA's rules.

260 Also, the FUMA pipeline sorted out a set of candidate SNPs from our inputs
261 that meets one of two conditions, 1) the independent significant SNPs and 2) SNPs that
262 are linked to the independent significant SNPs (with LD $r^2 \geq 0.6$). For condition 2,
263 the SNPs can be from our imputed genotypes if p value below 0.05 or from the reference
264 panel of 1000G EAS. ANNOVAR was used to annotate the candidate SNPs (29).

265

266 **Functional annotation of the mapped genes**

267 DAVID online tool (30) was used to analyze the enrichment of Gene Ontology (GO)
268 biological processes and KEGG pathways for the coding genes mapped to the risk
269 loci.

270

271 **Gene mapping**

272 We used three gene-mapping strategies provided by FUMA (27), including positional,
273 expression quantitative trait locus (eQTL) and chromatin interaction. For positional

mapping, ANNOVAR annotations were used. The candidate SNPs were mapped to the nearest genes within a maximum 10 Kbp distance. For eQTL mapping, expression data of all tissue types in GTEv6, GTEv7, and GTEv8 (31) were used. We required False Discovery Rate (FDR) < 0.05 and p value <0.001 for a valid eQTL mapping. All chromatin interaction data in FUMA were used (32-35). The promoter was set to upstream 2000 bp to downstream 500 bp of transcriptional starting sites. We required FDR < 1e-6 for a valid chromatin interaction mapping.

Analysis of genome-wide mRNA expression data

We first extracted the genome-wide microarray and RNA-seq data of human mRNA expression from GEO/NCBI database. The mRNA data includes three subsets in maternal PTB, infant PTB and breast cancer (Additional file 1: Table S8). Based on the normalized expression data provided by the database, we analyzed differentially expressed genes (DEGs) between different conditions, including 1) PTB vs. normal term, 2) BPD or sepsis vs. infant without BPD or sepsis, and 3) breast cancer vs. control samples. For microarray platform-based data, we used the *limma* package in R programming language and conducted empirical Bayes moderated t-test. DEGs were detected with a fold change above 1.5 and p value below 0.05. For RNA-seq data with raw counts, we utilized the Edge-R method to identify DEGs. The DEGs are listed in Additional file 1: Table S9.

295 # Results

296 ## Benchmarking genotype imputation using the ultra-low coverage
297 sequencing data of 17,844 embryos and HG005

298 We estimated the accuracy of the imputed genotypes from the SNPs of chromosome 1
299 both called in our 17,844 samples and the known genotypes in HG005. The genotype
300 imputation was benchmarked according to 80 combinations of the 10-scale coverages
301 of HG005 with 8 sizes of our samples. A monotonic increase in accuracy with
302 sequencing coverage was observed (Fig. 2a), consistent with previous studies (2, 24).
303 The accuracy for sample size of 2,000 stayed at around 0.48 under all sequencing
304 coverages. But for a larger sample size of 16,000, its accuracy increased from 0.48 at
305 0.01x to 0.66 at 0.1x. This result suggests that at ultra-low coverages, increase in sample
306 size could obtain higher accuracy (Additional file 1: Table S1). In general, a lower
307 coverage with a larger sample size results in better performance than a higher coverage
308 with a smaller sample size. For example, the genotype accuracy at 0.05x with 14,000
309 samples versus 0.1x with 4,000 embryos was 0.61 versus 0.55. A larger sample number
310 is therefore more efficient in optimizing genotype imputation than increasing sequence
311 coverage. It is also noticed that at the two lowest coverages in our experiments, the
312 contribution of increasing sample size was not significant and the accuracy plateaued
313 at 0.52 (0.01x) and 0.55 (0.02x). Using the same datasets, we evaluated allele accuracy
314 that relaxed zygosity correctness from genotype accuracy. The corresponding
315 accuracies were much better (increased to 0.7 and higher) while maintaining the same
316 trend with increasing sample size and coverage (Fig. 2b). Therefore, when the

317 genotypes are incorrectly imputed for some SNPs, the non-reference allele could be
318 correctly detected.

319 We next examined several important quality metrics that are widely used to filter
320 falsely imputed genotypes. The INFO score of IMPUTE2 style (36) denotes the
321 certainty of an imputed genotype and has been accepted as a quality metric of
322 imputation. For a combination of 0.04x coverage with 16,000 samples, we
323 benchmarked ten different INFO score thresholds from 0.1 to 1.0 and detected
324 corresponding SNPs. As increase in the INFO scores, we observed a consistent increase
325 in genotype accuracy from ~0.60 to 0.99, but a rapid decrease in number of SNPs that
326 meet these thresholds (Fig. 3a). Thus, INFO score could act as an effective metric to
327 evaluate the accuracies at ultra-low coverage, but its thresholds should be meticulously
328 chosen in order to retain sufficient SNPs. Effect of MAF scores on genotype accuracy
329 of HG005 were then tested as a potential metric. We divided the genotyping results at
330 different sequencing coverages (sample size fixed to 16,000) into bins of MAF ranges
331 (0.01 MAF a bin) and calculated the genotype accuracy each bin. The genotype
332 accuracy increased rapidly from MAF 0 to 0.05 and reached a turning point at 0.05.
333 After this point, the accuracy became slow increasing (Fig. 3b). However, even for the
334 most common SNPs (MAF 0.4~0.5), the accuracy was converged at ~70%. The
335 accuracy of the two lowest coverages 0.01x and 0.02x fluctuated especially at low MAF
336 cutoffs. Because such fluctuation was not observed during INFO testing, MAF might
337 not be a reliable metric to change genotype accuracy at ultra-low coverage. In
338 subsequent analyses, we followed the common practice to use SNPs with MAF ≥ 0.01

339 for GWAS. Finally, we combined HWE *p*-values with INFO scores as a filter but
340 without losing too many SNPs. HWE *p*-values could evaluate the probability of the
341 imputed genotype at a certain SNP that is significantly different from the expectations
342 by Hardy-Weinberg Equilibrium. We summarized the genotype accuracy of different
343 combinations of INFO scores and HWE *p*-value cutoffs in Table 1. When INFO scores
344 were set above 0.4, the accuracies of genotype and allele were 70.0% and 83.4%,
345 respectively, with 48,176 SNPs left. The "INFO score ≥ 0.4 and HWE *p*-value >1e-6"
346 resulted in an increased accuracy 71.5%, with 28773 SNPs left. Thus, our GWAS
347 utilized this setting, "INFO score ≥ 0.4 and HWE *p*-value >1e-6" as filtering criteria.
348 To summarize our benchmarking results for future study on ulcWGS, we built a
349 regression model (Formula 1) to calculate the expected genotype accuracy using
350 sequencing coverage and sample size as inputs.

$$acc = 2.227 * c + 8.937e^{-6} * s + 0.494 \ \ (c \geq 0.01, s \geq 4000) \qquad (1)$$

351 where *acc* is the expected genotype accuracy, *c* denotes the sequencing coverage, *s*
352 denotes the sample size. The model has a r^2 of 0.874 (Additional file 3: Figure S2).
353

354 **GWAS of gestational ages using 1,744 born embryos**

355 With the solid foundation laid out in the previous section, we have obtained sufficient
356 good quality SNPs for GWAS. Among the 17,844 sequenced embryos, 1,744 were
357 transferred and gave birth to a baby. The gestational age of all 1,744 born embryos are
358 well documented and thus were chosen for biological associated study. We revised the
359 population SNP calling method used in Liu et al. (8). A total of 151,793,444 SNPs were
360 detected and of 141,718,305 are bi-allelic. The MAF spectrum bi-allelic novel and

361 known variants in dbSNPv150 (37), 1000G (28) and gnomAD (38) is shown in
362 Additional file 3: Figure S3a. The transitions/transversions ratio for "all bi-allelic SNPs"
363 and "bi-allelic SNPs known in dbSNPv150" were 3.05 and 3.58, respectively. Pearson
364 correlation coefficient of the non-reference AFs between the 301 Chinese samples in
365 1000G (so-called 1000G CHN (28)) and the corresponding SNPs obtained in our
366 dataset was 0.986 (Additional file 3: Figure S3b). This result supports a strong
367 correlation between the two datasets, and high confidence of the known variants used
368 in our analysis. We also performed genotype imputation at bi-allelic population SNPs
369 with MAF ≥ 0.01. Pearson correlation coefficient was 0.985, showing a high
370 consistency between the estimated AFs in population SNP calling and in imputation.

371 Three different whole genome amplification (WGA) methods and four different
372 sequencing platforms were used in the PGT dataset (Additional file 1: Table S2). It is
373 not uncommon that large number of samples may use multiple sequencing platforms
374 and WGA. Removing these unrelated covariates from GWAS as much as possible is
375 essential especially when the sequencing coverage is ultra-low. Such covariates should
376 be detected and disregarded in GWAS. We applied Principal Component Analysis (PCA)
377 to the imputed genotypes of SNPs with MAF ≥ 0.05 among all 17,844 embryo samples
378 (Additional file 2: Supplementary Methods, Additional file 3: Figure S4a). The first and
379 second principal components distinguish the differences of sequencing platforms
380 (Additional file 3: Figure S4b) and of WGA methods (Additional file 3: Figure S4c).
381 Therefore, we used the top eight principal components and eight other clinical records
382 as covariates in GWAS. PCA was also applied to the GWAS samples and the top

383 principal components were included in the subsequent analyses as covariates for
384 removing the biases.

385 We used the state-of-the-art one-stage GWAS strategy (39) to analyze the
386 1,107,198 imputed SNPs in the 1,744 transferred and born embryo samples with
387 complete follow-up records. The distribution of gestational ages shown in Additional
388 file 3: Figure S5 include 162 preterm deliveries (gestational age < 37 weeks), 42 early
389 preterm deliveries (gestational age <34 weeks), and 8 very early preterm deliveries
390 (gestational age <28 weeks). The gestational ages were standardized by z-score and
391 incorporated as a quantitative trait.

392 A total 1,107, 198 SNPs with imputed genotypes were selected for GWAS that
393 are in accord with, 1) MAF ≥ 0.01, 2) known in dbSNPv150, and 3) passed the filter
394 "INFO score ≥ 0.4 and HWE *p*-value >1e-6". The Q-Q plot shows a large deviation of
395 the observed p values from the null hypothesis (Additional file 3: Figure S6). The
396 linkage disequilibrium score regression (LDSC) software package (40) with 1000G
397 EAS reference was used to estimate $\lambda_{GC} = 0.992$, mean $\chi^2 = 1.012$. The LD score
398 regression intercept was 0.952, standard error = 0.021, indicating that the population
399 stratification and other factors were well-controlled. We identified 40 significant SNPs
400 satisfying Bonferroni-corrected significant levels of 4.515e-8. The Manhattan plot
401 shows the distribution of the detected SNPs cross all chromosomes (Fig. 4a, Additional
402 file 1: Table S3).

403 We used FUMA (27) pipeline for GWAS downstream analysis. First, FUMA
404 generated a set of candidate SNPs and the 11 independent SNPs (Additional file 1:

405 Table S4). By annotation, most of the SNPs are located and enriched in intergenic and
406 intronic regions (Fig. 4b), which is similar to the previous study (41). Specifically, there
407 are 11 SNPs located in exons (0.8% of total), and 4 of them are non-synonymous SNPs
408 (Additional file 1: Table S5). Additionally, we observed the distribution of regulatory
409 elements and chromatin states with the candidate SNPs (Additional file 3: Figure S7).
410 According to RegulomeDB scores assigned to each candidate SNP, 1.09% SNPs were
411 classified as likely to affect regulator binding (score 2a and 2b) and 0.21% as likely to
412 affect regulator binding and linked to expression of a gene target (score 1d and 1f).
413 These proportions of SNPs hold a relatively high likelihood to affect the regulatory
414 elements along noncoding regions. Second, we identified 11 leading SNPs from their
415 corresponding genomic risk loci by FUMA. Fig. 4e shows the DNA length, number of
416 SNPs and mapped genes of these risk loci. The zoom in locus plot of the 11 risk loci
417 are shown in Additional file 3: Figure S8. Of 4 risk loci were reported to be associated
418 with refractive astigmatism, adolescent idiopathic scoliosis, glomerular filtration rate,
419 among others, indicating a possible connection of these diseases or traits with PTB
420 (Additional file 1: Table S6).

421 By integrating strategies positional, eQTL and chromatin interaction mappings,
422 we identified a total of 166 genes mapped to the 11 risk loci, including 48 and 19 genes
423 from two and three strategies, respectively (Fig. 4c, Additional file 1: Table S7). There
424 were 24 genes detected within or less than 10 Kbp from the candidate SNPs and 7 of
425 them were shown in Fig. 4a based on the location of the genomic risk loci. Importantly,
426 *CNTLN* was reported as a PTB related gene (42), and *PIN1* involves inhibition of breast

427 cancer (43). A Circos plot shows the graphic distribution of the mapped genes via eQTL
428 and chromatin interaction, and their links with the genomic risk loci (Fig. 4d). The
429 breakdown of each chromosome is shown in Additional file 3: Figure S9. Even though
430 not within any risk loci, *CRHBP* was linked through chromatin interaction mapping to
431 two loci, chr5:75101342-75164623 and chr5:78251511-78271282. Enrichment
432 analysis of DEGs in 30 tissue types in GTEx v8 (44) exhibits significant overexpression
433 of the mapped genes in both ovary and uterus (Additional file 3: Figure S10a). The
434 gene-set enrichment analysis also indicates their association with the immune system,
435 breast cancer and transcriptional regulation (Additional file 3: Figure S10b).
436

437 **Association of the 166 mapped genes from GWAS with preterm birth,**
438 **infant disease and breast cancer**

439 GWAS of gestational age related PTB has been implicated in biological functions that
440 include immune response, inflammatory response, and coagulation factors (11, 45-47).
441 We compared our 166 mapped genes with reported PTB markers by collection of 8
442 published resources, here classed to 3 PTB sets, including dbPTB from Sheikh et al.
443 (48) and Uzun et al (49), PTB-merged from 5 data resources (10), and PNAS-identified
444 DEGs of PTB in 2019 (10). We found that *CRHBP, EMR1, ICAM1, MBL2, OXTR,* and
445 *THBS4* have been reported in at least 2 PTB sets. Specifically, *ICAM1* was present in
446 all 3 sets and 6 data resources, and both *CRHBP* and *OXTR* in 5 resources (Additional
447 file 1: Table S7). In addition, there were 8 genes overlapped with 1 PTB set (Fig. 5a).
448 This result pinpoints a relationship of the detected risk loci with PTB, and possible roles
449 of the overlapped genes in PTB. There are totally 1,930 genes reported as PTB-related;

450 however, only 50 were frequently recognized by at least 5 data resources, hereafter
451 referred to as PTB marker genes (Additional file 1: Table S7). The 50-PTB marker set
452 was significantly enriched with inflammatory and immune response related processes
453 or pathways (Fig. 5b). Similarly, those PTB genes that overlapped with 3 or 4 resources
454 mainly participate in the same biological functions. The PTB-related genes listed at Fig.
455 5a involve immune response (*EMR1, ICAM1, PTPRZ1* and *MBL2*), inflammatory
456 response (*CRHBP, ICAM1, PTPRZ1* and *MBL2*), coagulation (*MBL2*), apoptosis
457 (*PLAGL1*) and cell adhesion (*ICAM1* and *THBS4*), emphasizing their associations with
458 PTB.

459 To determine the relationship between the mapped genes and PTB, we first
460 analyzed the DEGs between maternal PTB and normal term birth based on six
461 published datasets of genome-wide gene expression (Additional file 1: Tables S8 and
462 S9). Significant overexpression of *CRHBP* and *OXTR* were identified in two datasets,
463 while overexpressed (*ICAM1, EGR2,* and *PLAGL1*) and underexpressed (*THBS4*)
464 genes were present in one dataset (Table 2). Another *DKK1* expressed higher levels
465 above 2.0-fold in two datasets, suggesting its importance in PTB. Then, we analyzed
466 four infant PTB datasets of gene expression, and found differentially increased
467 expression of *ICAM1, CRHBP, DKK1, EGR2,* and *PLAGL1,* consistent with maternal
468 PTB. In contrast, significantly underexpression of *THBS4, PIN1* and *GCNT4* was
469 commonly detected by maternal and infant subgroups (Table 2). It is also noticed that
470 *DNMT1* shows increased expression in both fetal and maternal groups (Table 2). DNA
471 methylation was suggested to involve generation of early PTB (10); however, the role

472 of *DNMT1* as a DNA methyltransferase in PTB has not been determined yet. This
473 analysis provides evidence that these mapped DEGs above including *DNMT1* are
474 associated with both maternal and infant PTB. Relatively, *OXTR* seems to be related to
475 only maternal factor. A heatmap of mRNA expression shows clustering of 6 expression
476 profile cross PTB and normal term conditions (Fig. 5c). Two clusters display distinct
477 expression patterns of these PTB genes.

478 It is well known that bronchopulmonary dysplasia (BPD) is the most common
479 respiratory disorder among children born preterm (50, 51). The pathogenesis of BPD
480 involves multiple prenatal and postnatal mechanisms affecting the development of
481 immature lung. Also, neonatal sepsis is associated with severe morbidity and mortality
482 during the neonatal stage. The incidence of late-onset sepsis increases with increase in
483 survival rate of preterm and low weight babies (52). Thus, we examined the possible
484 relationship of the 166 genes with infant BPD and sepsis by analyzing gene expression
485 data derived from samples of preterm infants (Additional file 1: Table S8). We first
486 identified differentially increased expression of *CRHBP, ICAM1* and *EGR2* under PTB
487 of maternal & infant and BPD conditions, but differentially decreased expression of
488 *DKK1* (Table 2). Under sepsis condition, differentially overexpressed *CNTLN, ICAM1,*
489 and *PLAGL1* in PTB were consistently observed. By contrast, *GCNT4* expression was
490 always significantly decreased under maternal and infant subpopulations. The gene
491 clustering shows diversity of gene expression across different samples with infant PTB;
492 however, these up-regulated genes were grouped together (Fig. 5d), supporting the idea
493 that BPD or sepsis induces the change in these PTB genes.

494 Breast cancer is one of the most frequently diagnosed malignancies observed
495 during pregnancy. It often presents characteristics of high malignancy and are hormone
496 receptor negative like Estrogen receptor (ER)-, HER2+ or triple negative breast cancer
497 (TNBC). We collected gene expression data mainly presenting three subtypes of breast
498 cancer, TNBC, HER2+ and ER or Progesterone receptor (PR) (Additional file 1: Table
499 S8). By analysis of DEGs, we detected the expression of PTB related genes *DKK1,*
500 *ICAM1, DKK1, EGR2, PLAGL1, GCNT4* and *THBS4* in all three subtypes. Increased
501 *ICAM1* and decreased *PLAGL1* were consistently identified in these datasets (Table 2).
502 In fact, *ICAM1* has been reported as TNBC markers (53) and acts as prognostic
503 molecule of breast cancer (54). Both *ICAM1* and *DKK1* could increase expression in
504 TNBC cells (55). However, other PTB related genes do not display similar changes in
505 expression under the cancer subtypes. For example, *OXTR* was detected by only one
506 dataset of ER+/-, while *CRHBP, EMR1, PIN1* and *MBL2* were not found among any of
507 the subtypes. Conversely, underexpression of *PLAGL1* and *GCNT4* were found in all
508 three types of breast cancer. In addition, overexpression of *DNMT1* was observed in
509 TNBC and HER2+ subtypes, that validates its oncogenic roles in breast cancer and drug
510 target of TNBC (56, 57).

511 To identify further interactions between the selected PTB genes from Table 2 and
512 the top 50 PTB markers, we calculated Pearson correlation coefficient by comparing
513 their gene expression of maternal and infant PTB, BPD and sepsis subsets, respectively.
514 We built the corresponding co-expression networks of the PTB genes (Additional file
515 3: Figure S11). Clearly, the co-expressed genes involve immune and inflammatory

516 responses, coagulation, as well as apoptosis, angiogenesis, among others. We then
517 constructed the networks cross different subpopulations. As shown in Fig. 6a, the PTB
518 genes could involve both maternal and infant PTB processes, especially *ICAM1*,
519 *PLAGL1, EGR2* and *CRHBP* that link to TLR4, a known preterm marker associated
520 with immune and inflammatory processes (58). Similarly, co-expression interactions of
521 these genes with the top PTB markers were observed under maternal PTB and infant
522 BPD (Fig. 6b). Both *OXTR* and *PIN1* only display gene correlations under maternal
523 PTB, whereas *MBL2* only correlates under infant PTB. This analysis indicates that the
524 predicted PTB-related genes including *ICAM1*, *CRHBP*, *PLAGL1, EGR2, CNTLN,* and
525 *DKK1*, play an important role in preforming biological activities associated with PTB,
526 infant disease, possibly breast cancer, due to the gestational age-induced.
527

528 ## Discussion

529 Low or very low coverage sequencing data have been increasingly used in discovery of
530 genetic variation and GWAS. However, if the coverages are further decreased to
531 extremely ultra-low levels, how many samples are required to obtain a relatively high
532 accuracy of genotype, and whether these samples can be appropriately applied to
533 GWAS. To address this challenge, we used 17,844 PGT datasets of embryo samples
534 with an average of 0.04x coverage and achieved genotype imputation performance
535 comparable to those using low coverage samples. We first demonstrate that increase in
536 number of ulcWGS samples is more efficient than changing sequencing coverages and
537 indicates the ability of such ultra-low coverage PGT samples to obtain adequate
538 accuracy of phenotypes. Furthermore, we found that INFO score and HWE *p*-value are

539 effective to act as filters to improve the accuracy at ultra-low coverages while
540 meanwhile keep enough SNPs for downstream analyses. To our best knowledge, the
541 samples used in this study hold the lowest average WGS coverage for GWAS so far,
542 and our study provides a framework for guiding other researchers who work on
543 ulcWGS data.

544 Gestational age is a multi-factor phenotype involved in maternal and fetal
545 biological activities (59). To investigate effects of the fetal genome on gestational age,
546 we used the imputed genotypes of 1,744 born embryo samples, a cohort of samples who
547 successfully gave birth after *in vitro* fertilization. From the 166 genes mapped to the 11
548 genomic risk loci, we identified a set of the PTB-related genes that were previously
549 reported (12, 59). *CRHBP, ICAM1,* and *OXTR* are primary representative genes
550 showing evidence of genetic association with gestational age among our samples.
551 *CRHBP* is an important gene in maternal and fetal gestation that could regulate the
552 pregnancy length by increasing/decreasing the concentration of CRH (60, 61). *ICAM1*
553 involves disease induced PTB during pregnancy (62-64). Oxytocin signaling is
554 mediated by Oxytocin receptor (*OXTR*), which is related to gestational age (65). We
555 validated these predicted PTB genes by analysis of DEGs from maternal and infant
556 PTB subpopulations.

557 PTB is neonatal birth occurring before 37 weeks of gestation age and is a leading
558 cause of infant morbidity and mortality. Understanding of genetic and molecular
559 mechanisms of PTB and its association with gestation duration is currently insufficient.
560 Recently, Zhang et al. reported replicable loci in six genes (*EBF1, EEFSEC, AGTR2,*

561 *WNT4, ADCY5* and *RAP2C*) associated with gestational duration (12). This study
562 identified 3 genes (*EBF1, EEFSEC* and *AGTR2*) strongly associated with PTB in a
563 European ancestry cohort of 43,568 women. However, we did not detect such 6 genes
564 from the reported PTB markers and only identified them as DEGs from few published
565 datasets of PTB. This could be due to the heterogeneous sources of samples used in
566 different PTB studies or be explained in part by the genetic complexity of incomplete
567 gestation induced PTB complications. Here, we collected almost 2,000 PTB-related
568 genes from previous PTB studies. The differences in study design, source and subtype
569 of samples, and statistical methods would be important factors that could account for
570 the diversity of PTB variants and genes among the various studies. Considering the
571 possible association of PTB with other traits, we compared differential gene programs
572 on multiple phenotypes between mother and infant reported in previous studies, and
573 demonstrated a high risk of *CRHBP, ICAM1, DNMT1, CNTLN, PLAGL1, DKK1* and
574 *EGR2* with PTB among our sample cohorts of Chinese or Eastern Asian ancestry. To
575 support this finding, we reconstructed co-expressive networks linking the PTB-related
576 genes in GWAS with the reported PTB markers. Indeed, the correlated PTB genes are
577 mainly involved in immune & inflammation related processes and signaling pathways,
578 as well as coagulation factors. Thus, these findings have biological implications for
579 dissecting genetic associations of gestational factors with disease or traits in different
580 human ancestries.

581 Pregnancy is associated with an increased risk of developing breast cancer (66).
582 Although several reports indirectly described relationship between breast cancer and

583 PTB (67), evidence is still lacking. To determine whether a correlation exists between
584 PTB women and breast cancer pathogenesis, we compared differential expression of
585 the PTB related genes in PTB samples and three subtypes of hormone receptor-related
586 breast cancer samples. Although several DEGs were found in both PTB and cancer
587 subtypes, their expression patterns are not consistent. It perhaps is because of different
588 subtype of samples derived from heterogeneous populations, as well as different
589 phenotypes involved in the analyses. Nevertheless, our data provides additional
590 evidence that PTB might be related with breast cancer hormone-related subtypes. A
591 graphic overview of our results is summarized in Fig. 6c. We proposed interplays of
592 gestational age with PTB, fetal disease and breast cancer. The representative PTB genes
593 *CRHBP, ICAM1, THBS4, DNMT1, CNTLN, PLAGL1, DKK1* and *EGR2* are likely
594 associated with these phenotypes by targeting immune and inflammatory response,
595 coagulation, and cell adhesion.

596 **Conclusions**

597 This study benchmarked the ability of ulcWGS to be used for genotype imputation. As
598 the first study using a large cohort of human embryo samples with ulcWGS, we
599 demonstrate its power and effectiveness in GWAS. We detected 40 significant SNPs
600 and 11 genomic risk loci that contains independent significant SNPs and are associated
601 with gestational age. From 166 genes mapped to the risk loci. We establish
602 interrelationships between the mapped genes and maternal or infant diseases and
603 provide insights into understanding the genetic associations of gestational ages. Our
604 findings should expand current GWAS related to gestational duration and preterm trait

605 by including Chinese and East Asian samples and would therefore be helpful to future
606 research.
607
608 **Supplementary Information**
609
610 **Additional file 1: Table S1.** Genotype imputation performance at different ultra-low
611 coverages and sample sizes. **Table S2**. WGA methods and sequencing platforms used
612 in the PGT experiments. **Table S3**. The summary of 40 significant SNPs satisfying
613 Bonferroni-corrected significant levels of 4.526e-8 from 1,744 embryo PGT samples.
614 **Table S4**. The list of candidate SNPs. **Table S5**. Nonsynonymous SNPs that are
615 independent significant SNPs or in LD (r2>0.6) with one of the independent significant
616 SNPs. **Table S6**. The reported genomic risk loci from GWAS catalog that were detected
617 in our dataset. **Table S7**. A list of 166 mapped genes by positional, eQTL, and chromatin
618 interaction mappings. **Table S8**. Data sources of genome-wide mRNA expression in
619 Preterm birth, infant disease and breast cancer. **Table S9**. A list of the 166 mapped genes
620 that were also identified by differentially expressed genes (DEGs) derived from
621 analyzing the genome-wide gene expression datasets listed.
622 **Additional file 2: Supplemental Methods**
623 **Additional file 3: Figure S1.** Sequencing coverage statistics of the 17,844 embryos.
624 **Figure S2.** Visualizing the linear regression model for genotype accuracy prediction.
625 **Figure S3.** Quality control of SNP calling. Figure S4. Figure S4. Principal component
626 analysis of all 17,844 embryo samples. **Figure S5.** Distribution of gestational age in the

627 1,744 born embryo samples. **Figure S6.** Quantile-Quantile plot of the 1,107,198 studied
628 SNPs. **Figure S7.** Pie charts of the candidate SNPs. **Figure S8.** Zoom in locus plots of
629 the 11 genomic risk loci. **Figure S9.** Circos plots of chromatin interactions and eQTL
630 mapping. **Figure S10.** Gene set analysis of the 166 mapped genes. **Figure 11.** Co-
631 expression network of PTB-related genes in maternal and infant subtypes.
632

633 ### Abbreviations

634 WGS: whole genome sequencing; NGS: next-generation sequencing; GWAS:
635 genome-wide association study; bp: base pair; SNP: single nucleotide polymorphism;
636 PTB: preterm birth; PGT: preimplantation genetic testing; MAF: minor allele
637 frequency; LD: linkage disequilibrium; HWE: Hardy-Weinberg equilibrium; WGA:
638 whole genome amplification; PCA: principal component analysis; eQTL: expression
639 quantitative trait locus; FDR: false discovery rate; GO: gene ontology; BPD:
640 bronchopulmonary dysplasia; ER: Estrogen receptor; PR: Progesterone receptor;
641 HER2: human epidermal growth factor receptor 2; TNBC: Triple-negative breast
642 cancer; DEG: differentially expressed gene; AF: allele frequency. GIAB: Genome in a
643 Bottle; BWA: Burrows-Wheeler Aligner. GEO: Gene Expression Omnibus: NCBI:
644 National Center for Biotechnology Information.
645

646 ## Declarations

647 ### Ethics approval and consent to participate

648 All individual samples in the technical concordance cohort and clinical cohort, and
649 protocols used in this study have been reviewed and approved by the Institutional

Review Board (IRB) of China International Trust Investment Corporation - Xianngya (IRB Reference No. LL-SC-2020-004). The need to obtain informed consent has been waived by the IRB due to the study's retrospective nature. Following the regulations of the Human Genetic Resources Administration of China, all genetic materials involved in this study have been reviewed and approved by Ministry of Science and Technology of the People´s Republic of China (Approval No. [2022] GH1831). The experimental methods were in accordance with the principles of the Helsinki Declaration.

Consent for publication

Not applicable

Availability of data and materials

The datasets supporting the conclusions of this article are included within the article and its additional files. The significant SNPs and candidate SNPs are listed in Additional file 1: Tables S3 and S4, respectively. The processed or raw counts of mRNA expression datasets shown in Additional file 1: Table S8 was downloaded from Gene Expression Omnibus (GEO)/National Center for Biotechnology Information (NCBI).

Funding

The study was supported by the Early Career Schema (27204518) of the Hong Kong Research Grants Council for RL, partially by General Research Funding of Hong Kong Research Grants Council (17113721) for RL and (17117918) for BY, by the University

Grants Committees Fund from the University of Hong Kong for RL, partially by National Key Research and Developmental Program of China (2018YFC1004900) for YT, by the Innovation and Technology Fund (ITF/331/17FP) of Innovation and Technology Commission of the Hong Kong SAR government for TL.

Competing interests

The authors declare that they have no competing interests.

Authors' contributions

SL, RL and BY developed the computational pipeline and the algorithms. RL, GL, YW, TKL, and TL designed the experiments. PX, YG, FG and YT contributed to the clinical data collection. SL, BY, JL, YG and FG performed data processing and analysis. RL, GL, SL, BY, PX and YW participated in drafting the manuscript. All authors read and approved the final manuscript.

Acknowledgements

Not applicable

Reference

1. Visscher PM, Wray NR, Zhang Q, Sklar P, McCarthy MI, Brown MA, et al. 10 Years of GWAS Discovery: Biology, Function, and Translation. American journal of human genetics. 2017;101(1):5-22.
2. Pasaniuc B, Rohland N, McLaren PJ, Garimella K, Zaitlen N, Li H, et al. Extremely low-coverage sequencing and imputation increases power for genome-wide association studies. 2012;44(6):631.
3. Wang Z, Chatterjee N. Increasing mapping precision of genome-wide association studies: to genotype and impute, sequence, or both? Genome Biology. 2017;18(1):118.
4. Quick C, Anugu P, Musani S, Weiss ST, Burchard EG, White MJ, et al. Sequencing and imputation in GWAS: Cost-effective strategies to increase power and genomic coverage across diverse populations. 2020;44(6):537-49.
5. Gilly A, Southam L, Suveges D, Kuchenbaecker K, Moore R, Melloni GEM, et al. Very low-depth whole-genome sequencing in complex trait association studies. Bioinformatics. 2019;35(15):2555-61.
6. Homburger JR, Neben CL, Mishne G, Zhou AY, Kathiresan S, Khera AV. Low coverage whole genome sequencing enables accurate assessment of common variants and calculation of genome-wide polygenic scores. Genome medicine. 2019;11(1):74.
7. Marchini J, Howie B. Genotype imputation for genome-wide association studies. Nature reviews Genetics. 2010;11(7):499-511.
8. Liu S, Huang S, Chen F, Zhao L, Yuan Y, Francis SS, et al. Genomic Analyses from Non-invasive Prenatal Testing Reveal Genetic Associations, Patterns of Viral Infections, and Chinese Population History. Cell. 2018;175(2):347-59.e14.
9. Cronin FM, Segurado R, McAuliffe FM, Kelleher CC, Tremblay RE. Gestational Age at Birth and 'Body-Mind' Health at 5 Years of Age: A Population Based Cohort Study. PloS one. 2016;11(3):e0151222.
10. Knijnenburg TA, Vockley JG, Chambwe N, Gibbs DL, Humphries C, Huddleston KC, et al. Genomic and molecular characterization of preterm birth. Proceedings of the National Academy of Sciences of the United States of America. 2019;116(12):5819-27.
11. Liu X, Helenius D, Skotte L, Beaumont RN, Wielscher M, Geller F, et al. Variants in the fetal genome near pro-inflammatory cytokine genes on 2q13 associate with gestational duration. Nature communications. 2019;10(1):3927.
12. Zhang G, Feenstra B, Bacelis J, Liu X, Muglia LM, Juodakis J, et al. Genetic Associations with Gestational Duration and Spontaneous Preterm Birth. The New England journal of medicine. 2017;377(12):1156-67.
13. Wadon M, Modi N, Wong HS, Thapar A, O'Donovan MC. Recent advances in the genetics of preterm birth. Annals of human genetics. 2019.
14. Brezina PR, Kutteh WH, Bailey AP, Ke RW. Preimplantation genetic screening (PGS) is an excellent tool, but not perfect: a guide to counseling patients considering PGS. Fertil Steril. 2016;105(1):49-50.
15. Huang L, Bogale B, Tang Y, Lu S, Xie XS, Racowsky C. Noninvasive preimplantation genetic testing for aneuploidy in spent medium may be more reliable

than trophectoderm biopsy. Proc Natl Acad Sci U S A. 2019;116(28):14105-12.
16. Tan Y, Yin X, Zhang S, Jiang H, Tan K, Li J, et al. Clinical outcome of preimplantation genetic diagnosis and screening using next generation sequencing. GigaScience. 2014;3(1):30.
17. Zook JM, Chapman B, Wang J, Mittelman D, Hofmann O, Hide W, et al. Integrating human sequence data sets provides a resource of benchmark SNP and indel genotype calls. Nature Biotechnology. 2014;32(3):246-51.
18. Quinlan AR. BEDTools: The Swiss-Army Tool for Genome Feature Analysis. Current protocols in bioinformatics. 2014;47:11.2.1-34.
19. Li H, Durbin R. Fast and accurate short read alignment with Burrows–Wheeler transform. Bioinformatics. 2009;25(14):1754-60.
20. Li H, Handsaker B, Wysoker A, Fennell T, Ruan J, Homer N, et al. The Sequence Alignment/Map format and SAMtools. Bioinformatics. 2009;25(16):2078-9.
21. Li H. FermiKit: assembly-based variant calling for Illumina resequencing data. Bioinformatics. 2015;31(22):3694-6.
22. Kent WJ, Sugnet CW, Furey TS, Roskin KM, Pringle TH, Zahler AM, et al. The human genome browser at UCSC. Genome Res. 2002;12(6):996-1006.
23. Kent WJ, Zweig AS, Barber G, Hinrichs AS, Karolchik D. BigWig and BigBed: enabling browsing of large distributed datasets. Bioinformatics. 2010;26(17):2204-7.
24. Davies RW, Flint J, Myers S, Mott R. Rapid genotype imputation from sequence without reference panels. Nature genetics. 2016;48(8):965-9.
25. Skotte L, Korneliussen TS, Albrechtsen A. Association testing for next-generation sequencing data using score statistics. Genet Epidemiol. 2012;36(5):430-7.
26. Korneliussen TS, Albrechtsen A, Nielsen R. ANGSD: Analysis of Next Generation Sequencing Data. BMC Bioinformatics. 2014;15:356.
27. Watanabe K, Taskesen E, van Bochoven A, Posthuma D. Functional mapping and annotation of genetic associations with FUMA. Nature communications. 2017;8(1):1826.
28. Auton A, Brooks LD, Durbin RM, Garrison EP, Kang HM, Korbel JO, et al. A global reference for human genetic variation. Nature. 2015;526(7571):68-74.
29. Wang K, Li M, Hakonarson H. ANNOVAR: functional annotation of genetic variants from high-throughput sequencing data. Nucleic Acids Res. 2010;38(16):e164.
30. Sherman BT, Hao M, Qiu J, Jiao X, Baseler MW, Lane HC, et al. DAVID: a web server for functional enrichment analysis and functional annotation of gene lists (2021 update). Nucleic Acids Res. 2022.
31. The Genotype-Tissue Expression (GTEx) project. Nat Genet. 2013;45(6):580-5.
32. Schmitt AD, Hu M, Jung I, Xu Z, Qiu Y, Tan CL, et al. A Compendium of Chromatin Contact Maps Reveals Spatially Active Regions in the Human Genome. Cell reports. 2016;17(8):2042-59.
33. Giusti-Rodriguez PM, Sullivan PF. Using three-dimensional regulatory chromatin interactions from adult and fetal cortex to interpret genetic results for psychiatric disorders and cognitive traits. 2019:406330.
34. Akbarian S, Liu C, Knowles JA, Vaccarino FM, Farnham PJ, Crawford GE, et al. The PsychENCODE project. Nature neuroscience. 2015;18(12):1707-12.

35. Noguchi S, Arakawa T, Fukuda S, Furuno M, Hasegawa A, Hori F, et al. FANTOM5 CAGE profiles of human and mouse samples. Scientific data. 2017;4:170112.
36. Howie BN, Donnelly P, Marchini J. A flexible and accurate genotype imputation method for the next generation of genome-wide association studies. PLoS Genet. 2009;5(6):e1000529.
37. Sherry ST, Ward MH, Kholodov M, Baker J, Phan L, Smigielski EM, et al. dbSNP: the NCBI database of genetic variation. Nucleic Acids Res. 2001;29(1):308-11.
38. Karczewski KJ, Francioli LC, Tiao G, Cummings BB, Alföldi J, Wang Q, et al. The mutational constraint spectrum quantified from variation in 141,456 humans. Nature. 2020;581(7809):434-43.
39. Skol AD, Scott LJ, Abecasis GR, Boehnke M. Joint analysis is more efficient than replication-based analysis for two-stage genome-wide association studies. Nat Genet. 2006;38(2):209-13.
40. Bulik-Sullivan BK, Loh PR, Finucane HK, Ripke S, Yang J, Patterson N, et al. LD Score regression distinguishes confounding from polygenicity in genome-wide association studies. Nat Genet. 2015;47(3):291-5.
41. Maurano MT, Humbert R, Rynes E, Thurman RE, Haugen E, Wang H, et al. Systematic localization of common disease-associated variation in regulatory DNA. Science. 2012;337(6099):1190-5.
42. Pasaniuc B, Rohland N, McLaren PJ, Garimella K, Zaitlen N, Li H, et al. Extremely low-coverage sequencing and imputation increases power for genome-wide association studies. Nature Genetics. 2012;44:631.
43. Wulf G, Ryo A, Liou Y-C, Lu KP. The prolyl isomerase Pin1 in breast development and cancer. Breast Cancer Res. 2003;5(2):76-82.
44. Consortium GT. The GTEx Consortium atlas of genetic regulatory effects across human tissues. Science (New York, NY). 2020;369(6509):1318-30.
45. Vora B, Wang A, Kosti I, Huang H, Paranjpe I, Woodruff TJ, et al. Meta-Analysis of Maternal and Fetal Transcriptomic Data Elucidates the Role of Adaptive and Innate Immunity in Preterm Birth. Front Immunol. 2018;9:993-.
46. Strauss JF, 3rd, Romero R, Gomez-Lopez N, Haymond-Thornburg H, Modi BP, Teves ME, et al. Spontaneous preterm birth: advances toward the discovery of genetic predisposition. American journal of obstetrics and gynecology. 2018;218(3):294-314.e2.
47. Velez DR, Fortunato SJ, Thorsen P, Lombardi SJ, Williams SM, Menon R. Preterm birth in Caucasians is associated with coagulation and inflammation pathway gene variants. PloS one. 2008;3(9):e3283-e.
48. Sheikh IA, Ahmad E, Jamal MS, Rehan M, Assidi M, Tayubi IA, et al. Spontaneous preterm birth and single nucleotide gene polymorphisms: a recent update. BMC Genomics. 2016;17(Suppl 9):759.
49. Uzun A, Sharma S, Padbury J. A bioinformatics approach to preterm birth. American journal of reproductive immunology (New York, NY : 1989). 2012;67(4):273-7.
50. Siffel C, Kistler KD, Lewis JFM, Sarda SP. Global incidence of bronchopulmonary

dysplasia among extremely preterm infants: a systematic literature review. The journal of maternal-fetal & neonatal medicine : the official journal of the European Association of Perinatal Medicine, the Federation of Asia and Oceania Perinatal Societies, the International Society of Perinatal Obstet. 2019:1-11.
51. Cai Y, Ma F, Qu L, Liu B, Xiong H, Ma Y, et al. Weighted Gene Co-expression Network Analysis of Key Biomarkers Associated With Bronchopulmonary Dysplasia. Front Genet. 2020;11:539292.
52. Villamor-Martinez E, Lubach GA, Rahim OM, Degraeuwe P, Zimmermann LJ, Kramer BW, et al. Association of Histological and Clinical Chorioamnionitis With Neonatal Sepsis Among Preterm Infants: A Systematic Review, Meta-Analysis, and Meta-Regression. Front Immunol. 2020;11:972.
53. Rosette C, Roth RB, Oeth P, Braun A, Kammerer S, Ekblom J, et al. Role of ICAM1 in invasion of human breast cancer cells. Carcinogenesis. 2005;26(5):943-50.
54. Schroder C, Witzel I, Muller V, Krenkel S, Wirtz RM, Janicke F, et al. Prognostic value of intercellular adhesion molecule (ICAM)-1 expression in breast cancer. J Cancer Res Clin Oncol. 2011;137(8):1193-201.
55. Xu WH, Liu ZB, Yang C, Qin W, Shao ZM. Expression of dickkopf-1 and beta-catenin related to the prognosis of breast cancer patients with triple negative phenotype. PloS one. 2012;7(5):e37624.
56. Shin E, Lee Y, Koo JS. Differential expression of the epigenetic methylation-related protein DNMT1 by breast cancer molecular subtype and stromal histology. J Transl Med. 2016;14:87.
57. Wong KK. DNMT1: A key drug target in triple-negative breast cancer. Semin Cancer Biol. 2020.
58. Robertson SA, Hutchinson MR, Rice KC, Chin PY, Moldenhauer LM, Stark MJ, et al. Targeting Toll-like receptor-4 to tackle preterm birth and fetal inflammatory injury. Clin Transl Immunology. 2020;9(4):e1121.
59. Zhang G, Srivastava A, Bacelis J, Juodakis J, Jacobsson B, Muglia LJ. Genetic studies of gestational duration and preterm birth. Best Pract Res Clin Obstet Gynaecol. 2018;52:33-47.
60. Petraglia F, Imperatore A, Challis JR. Neuroendocrine mechanisms in pregnancy and parturition. Endocr Rev. 2010;31(6):783-816.
61. Majzoub JA, McGregor JA, Lockwood CJ, Smith R, Taggart MS, Schulkin J. A central theory of preterm and term labor: putative role for corticotropin-releasing hormone. American journal of obstetrics and gynecology. 1999;180(1 Pt 3):S232-41.
62. Díaz-Pérez FI, Hiden U, Gauster M, Lang I, Konya V, Heinemann A, et al. Post-transcriptional down regulation of ICAM-1 in feto-placental endothelium in GDM. Cell adhesion & migration. 2016;10(1-2):18-27.
63. Chen X, Scholl TO. Maternal biomarkers of endothelial dysfunction and preterm delivery. PloS one. 2014;9(1):e85716.
64. Labarrere CA, Bammerlin E, Hardin JW, Dicarlo HL. Intercellular adhesion molecule-1 expression in massive chronic intervillositis: implications for the invasion of maternal cells into fetal tissues. Placenta. 2014;35(5):311-7.
65. Kim SC, Lee JE, Kang SS, Yang HS, Kim SS, An BS. The regulation of oxytocin

and oxytocin receptor in human placenta according to gestational age. Journal of molecular endocrinology. 2017;59(3):235-43.
66. Keyser EA, Staat BC, Fausett MB, Shields AD. Pregnancy-associated breast cancer. Rev Obstet Gynecol. 2012;5(2):94-9.
67. Froehlich K, Schmidt A, Heger JI, Al-Kawlani B, Aberl CA, Jeschke U, et al. Breast cancer, placenta and pregnancy. Eur J Cancer. 2019;115:68-78.

906 # Figures

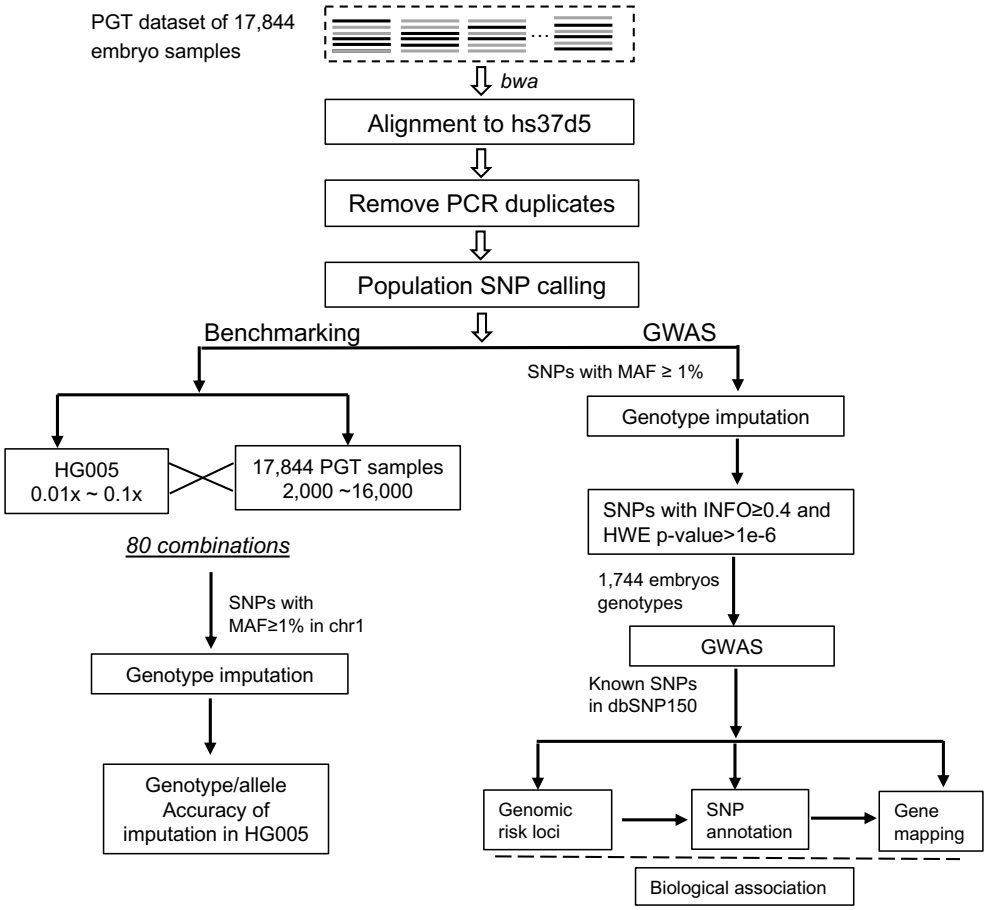

907

908 **Fig. 1. An overview of the analysis and benchmarking pipeline for ultra-low**
909 **coverage WGS.**

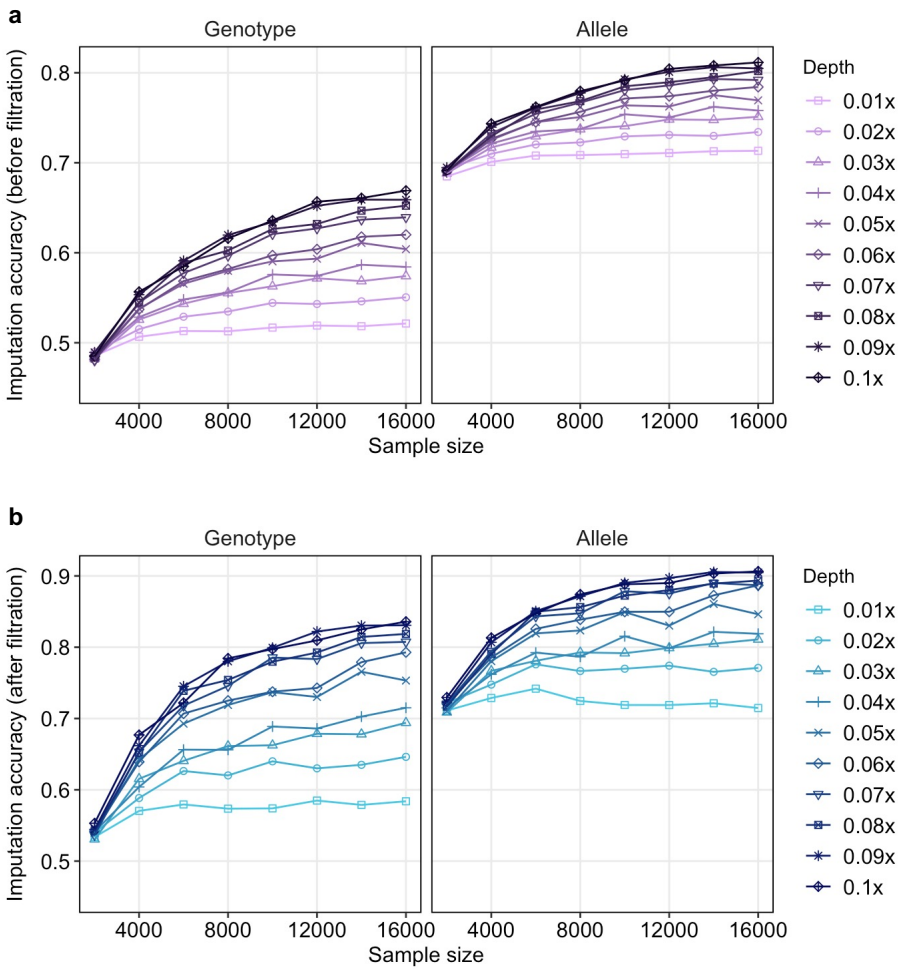

Fig. 2. Imputation accuracy at different coverages and sample sizes. The accuracies of imputed genotype (a) or allele (b) were obtained by comparing with the known genotypes in HG005. After using filter "INFO score ≥ 0.4 and HWE *p*-value > 1e-6", the accuracies of imputed genotype (c) or allele (d).

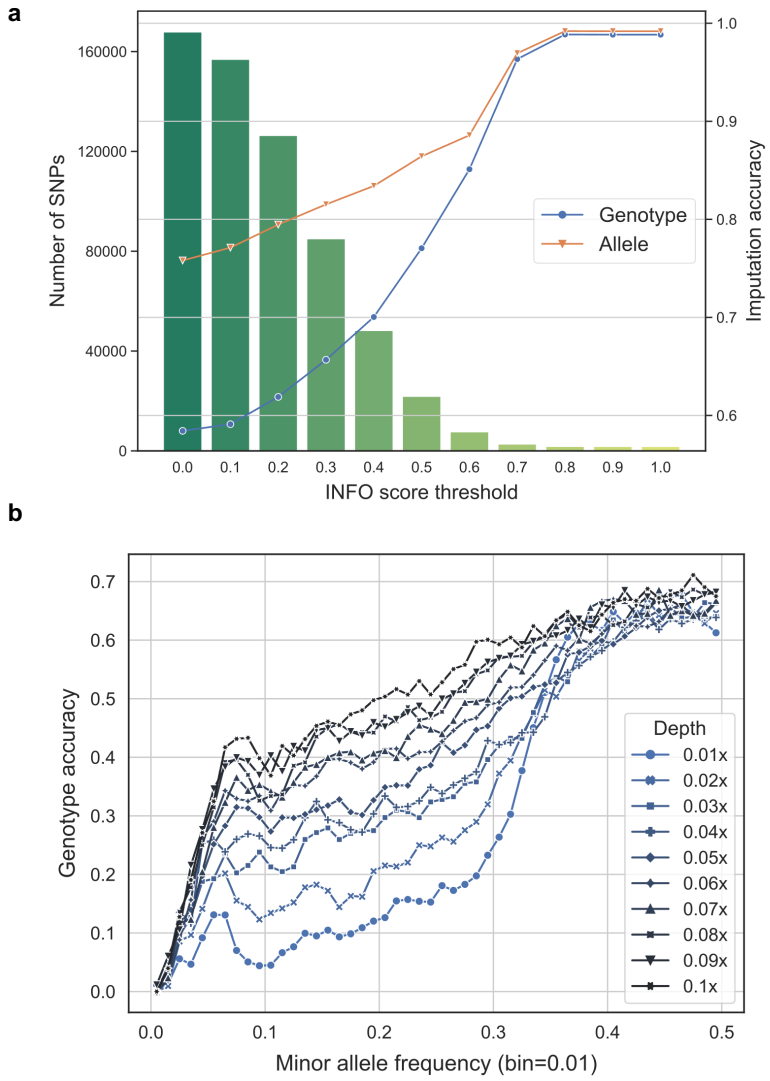

Fig. 3. Performance of different imputation result filters. The accuracies of our samples were calculated against the known genotypes in HG005. a, effect of INFO score filtering cutoffs on genotype and allele accuracies. The imputation was conducted by using 0.04x sequencing coverage of HG005 and with 16000 embryo samples. b, effect of MAF cutoffs on genotype accuracy at multiple sequencing coverages. The imputation was conducted through different sequencing coverages of HG005 with 16000 embryo samples.

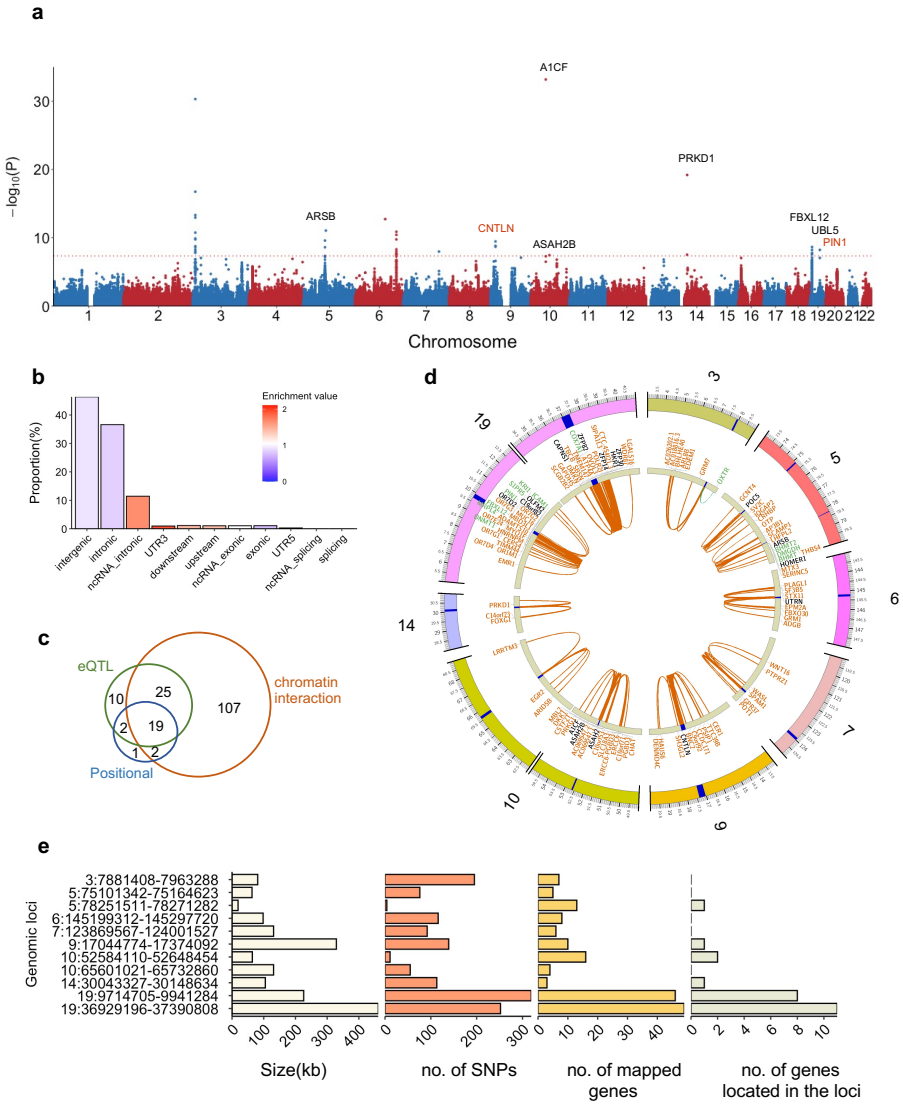

Fig. 4. SNP-based genome-wide association on gestational age. a, Manhattan plot of the SNPs in GWAS. The red dash line represents the genome-wide significance level 4.515e-8. The SNP "rs946934582" with p value of 2.764e-144 is beyond the scale, thus hereby listed alone. The genes shown are linking with the candidate SNPs and position of the corresponding genomic risk loci. b, functional annotation and enrichment test result of the candidate SNPs in FUMA. c, a Venn diagram of the 166 genes that could be mapped to the 11 genomic risk loci by positional, eQTL and chromatin interaction strategies. d, a Circos plot of the chromatin interactions and eQTL mapping in the 11 genomic risk loci from eight chromosomes. The outer ring is chromosomes, the regions in blue denote genomic risk loci. The middle ring represents the mapped genes. The color of the gene symbols shows how they were mapped, eQTL in green, chromatin interaction in orange, and both eQTL and chromatin interaction in black. The inner ring shows the linking edges, eQTL in green, and chromatin interaction in orange. e, a summary of the 11 genomic risk loci.

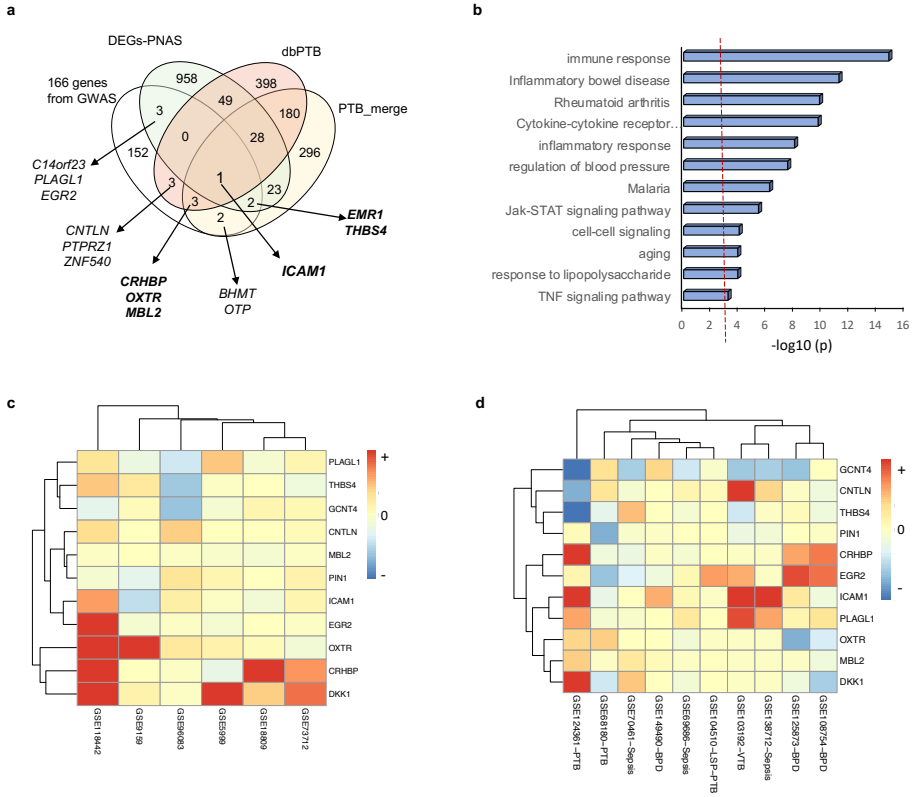

Fig. 5. Comparison of the 166 genes mapped to 11 genomic risk loci with PTB and infant disease. a, the 166 mapped genes were compared with 3 sets of reported PTB genes including dbPTB from Sheikh et al. (48) and Uzun et al (49), PTB-merged from 5 resources (10), and PNAS-identified DEGs in 2019 (10) (see Additional file 1: Table S8). b, a bar graph showing significantly enriched GO biological processes and KEGG pathways based on the 50 PTB marker genes (see Additional file 1: Table S7). c-d, heatmaps showing expression profiling and clusters of the PTB genes predicted from GWAS under maternal PTB (c) and PTB infant with BPD and sepsis (d). The gene expression data was extracted from the listed GSE accession numbers of NCBI/GEO.

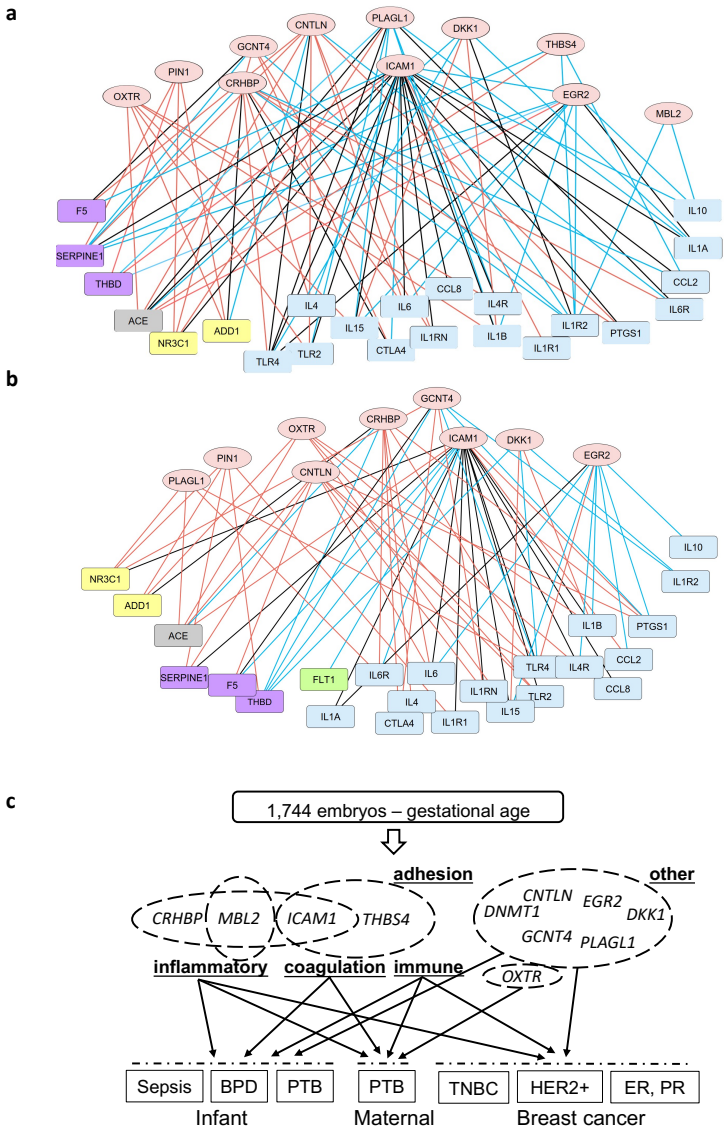

Fig. 6. Associated analysis of the PTB-related genes in maternal and infant subtypes. a, a gene co-expression network merging maternal and infant PTB subtypes. b, a gene co-expression network merging maternal PTB and BPD of preterm infant. In A and B, oval nodes represent PTB related genes predicted from GWAS using the 1,744 born embryo samples, rectangle nodes refer to the 50 top PTB markers summarized from previously studies (Additional file 1: Table S7), involving immune or inflammation (blue), apoptosis (yellow), angiogenesis (green), coagulation (purple) and other biological processes (grey). Co-expressive edges (Pearson correlation p value < 0.01) linking nodes represent maternal (red), infant (blue) and both maternal and infant (black). c, a graphic summary to illustrate gestational age's association with PTB, infant disease and breast cancer.

969 **Table 1. Genotype imputation performance with different filtering criteria**

970

Filtering criteria	SNP number	Genotype accuracy	Allele accuracy
None	167814	0.584	0.758
Known SNP in 1000G reference panel	141161	0.578	0.751
INFO score ≥ 0.1	156835	0.591	0.771
INFO score ≥ 0.2	126331	0.618	0.794
INFO score ≥ 0.3	84932	0.656	0.815
INFO score ≥ 0.4	48176	0.7	0.834
MAF ≥ 0.05	162788	0.597	0.777
HWE *p*-value > 1e-9	84237	0.595	0.695
HWE *p*-value > 1e-6	77419	0.596	0.692
HWE *p*-value > 1e-3	65561	0.599	0.687
HWE *p*-value > 1e-6 and INFO score ≥ 0.1	68505	0.610	0.713
HWE *p*-value > 1e-6 and INFO score ≥ 0.2	55972	0.646	0.751
HWE *p*-value > 1e-6 and INFO score ≥ 0.3	42202	0.681	0.786
HWE *p*-value > 1e-6 and INFO score ≥ 0.4	28773	0.715	0.818

971 Totally 16,000 samples with an average of 0.04x sequencing coverage were used for imputation.

972

973 **Table 2. Main mapped genes differentially expressed in PTB, infant disease and**
974 **breast cancer**

975

Genes mapped to risk loci	Overlapped No. with the reported PTB datasets	No. of DEGs detected in gene expression data						
		Maternal PTB	Infant PTB	Infant BPD	Infant sepsis	Breast cancer ER, PR	Breast cancer TNBC	Breast cancer HER2+
ICAM1	6	1(up)	2(up)	1(up)	1(up)	1(up),2(down)	2(up)	1(up)
CRHBP	5	2(up)	1(up)	1(up)				
OXTR	5	2(up)				1(up)	1(down)	
THBS4	3	1(down)	1(down)		1(up)	1(up)	2(down)	1(up),1(down)
EGR2	2	1(up)	1(up)	1(up)		1(up)	2(down)	2(down)
CNTLN	1	1(up)	1(up),1(down)		1(up)	1(down)		1(down)
MBL2	4		1(up)					
EMR1	2			1(up)				
PLAGL1	1	1(up)	2(up)		1(up)	2(down)	2(down)	2(down)
DKK1		2(up)	1(up)	1(down)		2(down)	3(up),1(down)	1(up),1(down)
GCNT4		1(down)	2(down)	1(down)	2(down)	1(up),2(down)	1(down)	1(down)
DNMT1		1(up)	1(up)				1(up)	1(up)
PIN1		1(down)	1(down)					

976 PTB related genes identified in our GWAS were compared with DEGs identified in published gene
977 expression datasets (Additional file 1: Table S9). “up” and “down” indicate differentially overexpressed
978 and underexpressed gene, respectively.